Electromechanical Modeling of Hybrid Piezohydraulic Actuator System for Active Vibration Control

Punan Tang

Alan B. Palazzolo

Texas A&M University,
College Station, TX 77843-3123

Albert F. Kascak

Gerald T. Montague

U.S. Army at NASA Lewis,
21000 Brookpark Road,
Cleveland, OH 44135

Electromechanical modeling of a hybrid piezohydraulic actuator system for active vibration control was developed. The transfer function of piezoelectric actuator was derived from the electromechanical potential energy law. This transfer function represents the dynamic relationship between input electric voltage and piezoelectric actuator displacement. The hydraulic actuator was characterized by impedance matching in which its transfer functions were experimentally determined. The transfer functions were transformed into a state-space representation, which is easily assembled into an active vibration control (AVC) closed-loop simulation. Good correlation of simulation and test was achieved for the hybrid system. A closed-loop dynamic simulation for imbalance response with/without AVC of a spinning rotor test rig at NASA Lewis was performed and showed excellent agreement with test results. The simulation couples the piezoelectric, hydraulic, and structural (rotor) components.

Introduction

Piezoelectricity was discovered by Pierre and Jacques Curie in the 1880's. Since then, it has been applied in precision mechanics, mechanical engineering, optics and measuring technology, medicine, and microelectronics. Piezoelectricity is the property of a crystalline material that is able to produce changes in its dimensions in the direction of an electric field which is parallel to the material polarization direction. Rotorbearing systems occur in the machinery, aerospace, power utility and petrochemical industries. Rotorbearing systems usually operate at a wide range of rotating speeds to meet needs of high efficiency and power output. Vibrations are encountered when rotating speeds are close to critical speeds and may be suppressed by adding damping, shifting critical speeds or reducing the imbalance force by passive or active means. An active vibration control system consists mainly of sensors, controller (analog or digital), power amplifiers, and actuators which suppress the vibration by counteracting the sensed vibrations. Piezoelectric actuator and electromagnetic shakers are used as actuators due to their high frequency band, large stroke, and large force output.

Palazzolo et al. (1991) successfully applied a piezoelectric actuator to suppress imbalance, subsynchronus, and transient vibration on a rotor test rig. Desirable features for actuators in rotating systems include: compactness, high force and stroke capability, and high and low temperature operation. These requirements exist because some rotor systems such as jet and rocket engines have limited space. Tang and Palazzolo (1993a) developed a combined piezohydraulic actuator system and successfully applied it to active vibration control of a rotor test rig at NASA Lewis. Figure 1 shows the configuration of this hybrid actuator. This consists of an output piston driven remotely by a piezoelectric actuator. The hydraulic fluid in the transmission tube was a liquid plastic, in Tang and Palazzolo (1993a), that was specially formulated to reduce leakage. Dual "*O*" ring seal are also included on each piston for this purpose. An electromechanical model for this hybrid system is required for closed-loop dynamic simulation with active vibration control.

The piezoelectric model is based on a one-dimensional "Mason" equivalent circuit (Kossoff, 1966) with electric parameters (resistance, inductance, and capacitance). The basic input elements of this model are taken from measured data. Many authors have studied piezoelectric structure vibration models. Holland and Eer Nisse (1968) used the Rayleigh-Ritz method for treatment of mechanically free parallelepipedic rectangle with the main surface fully covered with electrodes. Allik (1974), and Tomikawa (1978) applied the three-dimensional finite element method to low frequency transducer computations and resonators. However, no complex transfer functions were given for expressing the electromechanical relationship between input voltage and output expansion. Lin (1990) used an ideal model which has a piezoelectricity and payload stiffness, and produces a tip displacement proportional to input voltage. This model is easy to assemble in the closed-loop AVC simulations; however, it is essentially a static model.

This paper presents a new modeling method for the piezohydraulic actuator system. A simplified version neglecting piezoelectric stack dynamic was presented in Tang, and Palazzolo (1993b) for imbalance response simulation with active vibration control (AVC). The current model is based on a transfer function of the piezoelectric actuator as derived from the potential energy law (Cade, 1946). This transfer function represents the relationship between input electric voltage and piezoelectric actuator displacement. A transfer function based approach is also employed for modeling the hydraulic actuator. This model employs experimentally derived frequency response functions.

Energy Equation for Piezoelectric Crystals

Neglecting thermal effects, the energy per unit volume of a piezoelectric material is (Cade, 1946);

$$P_v = \tfrac{1}{2}\,\boldsymbol{\sigma}^T\mathbf{S}^E\boldsymbol{\sigma} + \tfrac{1}{2}\,\mathbf{E}^T\mathbf{C}^\eta\mathbf{E} - \tfrac{1}{2}\,\mathbf{E}^T\mathbf{D}\boldsymbol{\sigma} \qquad (1)$$

Equation (1) may be rewritten as

$$P_v = V_v + W_v + Z_v \qquad (2)$$

Contributed by the Dynamic Systems and Control Division for publication in the JOURNAL OF DYNAMIC SYSTEMS, MEASUREMENT, AND CONTROL. Manuscript received by the Dynamic Systems and Control Division September 23, 1994; revised manuscript received January 8, 1996. Associate Technical Editor: W. Book.

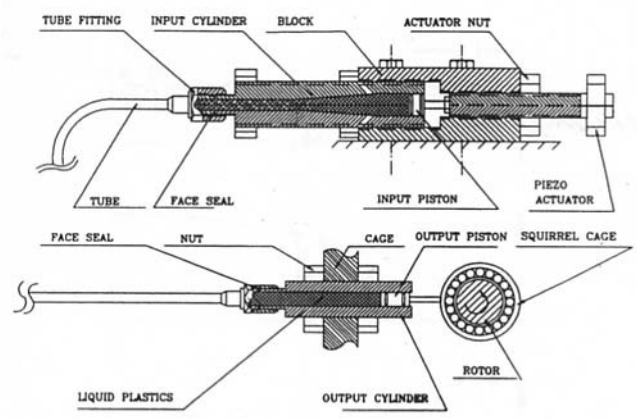

Fig. 1 Piezohydraulic actuator system

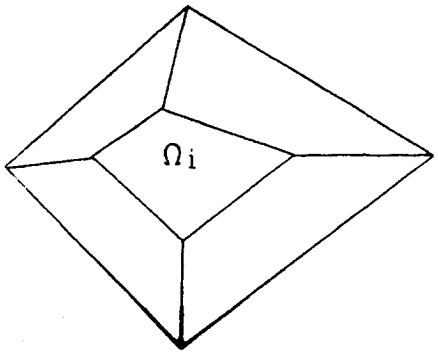

Fig. 2 Arbitrary piezoelectric crystal

where V_v is the mechanical energy density

$$V_v = \tfrac{1}{2}\,\boldsymbol{\sigma}^T \mathbf{S}^E \boldsymbol{\sigma} \tag{3}$$

W_v is the electric energy density

$$W_v = \tfrac{1}{2}\,\mathbf{E}^T \mathbf{C}^\eta \mathbf{E} \tag{4}$$

Z_v is the electromechanical energy density

$$Z_v = -\tfrac{1}{2}\,\mathbf{E}^T \mathbf{D} \boldsymbol{\sigma} \tag{5}$$

Piezoelectric Ceramic Total Energy

A piezoelectric actuator consists of numerous individual polycrystalline ceramic elements instead of natural piezoelectric crystals connected electrically in series/parallel. Figure 2 shows an arbitrary shape piezoelectric crystal. The total energy of this crystal according to Eq. (1) is

$$P_{vi} = \int_{\Omega i} V_{vi}\,d\Omega + \int_{\Omega i} W_{vi}\,d\Omega + \int_{\Omega i} Z_{vi}\,d\Omega \tag{6}$$

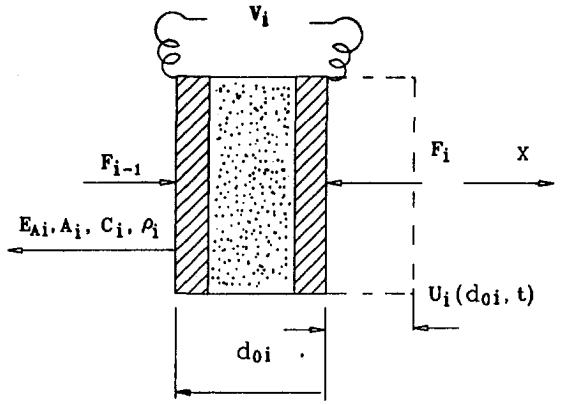

Fig. 3 Piezoelectric ceramic one-dimensional expansion under external voltage

Figure 3 shows the ith thin piezoelectric ceramic plate or disk in the overall stack. The ceramic plate or disk lies between two electrode surfaces, one of which is connected to the control voltage and the other to ground. The piezoelectric ceramic element, which has an electric field in its polarization direction expands in the x direction under external voltage V_i. By applying the following equations

$$d\Omega_i = A_i\,dx, \quad dm_i = \rho_i A_i\,dx,$$

$$\sigma_i = E_{Ai} u_i'(x, t) \quad \left(\text{where} \quad u_i'(x, t) = \frac{\partial u_i(x, t)}{\partial x}\right) \tag{7}$$

The elastic energy can be expressed by:

$$V_{Ti} = \int_{\Omega_i} V_{vi}\,d\Omega = \int_{x_i}^{x_i + d_{0i}} V_{vi} A_i\,dx$$

$$= \int_{x_i}^{x_i + d_{0i}} \tfrac{1}{2}\,E_{Ai} A_i (u_i'(x, t))^2\,dx \tag{8}$$

where

$$V_{vi} = \tfrac{1}{2}\,E_{Ai}(u_i'(x, t))^2 \tag{9}$$

The electric energy for one piezoelectric plate is (Crandall, 1990);

$$W_{Ti} = \frac{1}{2}\,\frac{q_i^2}{c_i(d_{0i} + u_i(x_i + d_{oi}, t))} = \frac{1}{2}\,\frac{q_i^2}{c_i(d_{0i})}$$

$$(d_{0i} \gg u_i(x_i + d_{oi}, t)) \tag{10}$$

Nomenclature

$\boldsymbol{\sigma}$ = stress vector (6×1)
$\mathbf{E}$ = electrical field vector (6×1)
P_v = energy density
$\mathbf{S}^E$ = elastic compliance vector (6×1)
$\mathbf{C}^\eta$ = dielectric susceptibility vector (6×1)
$\mathbf{D}$ = piezoelectric strain coefficient matrix (6×6)
E_{Ai} = elastic modulus of piezoelectric ceramic plate
A_i = cross-sectional area of the piezoelectricity ceramic plate
$u_i(x, t)$ = deflection in polarization direction
q_i = electric charge
d_{33} = piezoelectric charge constant in polarization direction
ρ_i = mass density of ceramic plate
d_{0i} = thickness of ceramic plate
$c_i(d_{0i})$ = capacitance, which is a function of the thickness of a ceramic plate
E_i = electric field strength
$\Phi_i(x)$ = ith mode shape
$w_i(t)$ = ith response function
δ = piezoelectric static expansion (m)
n = number of piezoelectric ceramic disks or plates
V = external DC voltage (V)

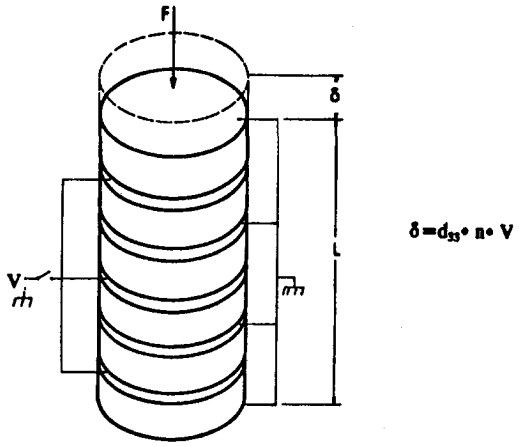

Fig. 4 "Free tip" static expansion of a stacked piezoelectric actuator

and the electromechanical energy is

$$Z_{Ti} = \int_{\Omega_i} - d_{33_i} E_i \sigma_i \, d\Omega$$

$$= -d_{33_i} E_i E_{A_i} A_i \int_{x_i}^{x_i + d_{0i}} u_i'(x, t) d\Omega \qquad (11)$$

By applying the following electric field strength relationship

$$E_i = \frac{q_i}{c_i d_{0i}} \qquad (12)$$

Eq. (11) can be written as

$$Z_{Ti} = -d_{33_i} \frac{q_i}{c_i d_{0i}} E_{A_i} A_i \int_{x_i}^{x_i + d_{0i}} u_i'(x, t) d\Omega \qquad (13)$$

and the kinetic energy for this piezoelectric ceramic element is

$$T_i = \frac{1}{2} \int_{\Omega_i} dm_i \dot{u}_i^2(x, t) = \frac{1}{2} \int_{x_i}^{x_i + d_{0i}} \rho_i A_i \dot{u}_i^2(x, t) dx \qquad (14)$$

Piezoelectric Actuator (Stacked Model)

The piezoelectric ceramic elements are assembled into a stacked form for a positioning actuator as shown in Fig. 4. This figure illustrates the free tip expansion of the stack subjected to a static voltage. The active part of positioning element consists of a stack of thin ceramic disks sandwiched between the metallic electrodes which are connected to external control voltage. Larger linear expansion can be achieved by making the disk thinner for a given operating voltage (the thinner the disk, the higher the field strength). Figure 5 shows a dynamic model of the piezoelectric positioning actuator which consists of hundreds of thin ceramic disks or plates. For this stack K_H is the external equivalent stiffness, which includes the payload spring stiffness and the external stiffness, m is the total mass of the piezoelectric crystals, m_e represents the mass of the actuator tip, C_H represents the equivalent external damping, and + or − indicates the direction of external voltage on the ceramic. The following assumptions are made for simplicity; geometry, external voltage, physical properties (mass density, elastic modulus), electrical properties (resistance, capacitance, inductance) are the same and constant for all the ceramic disks or plates. Hence;

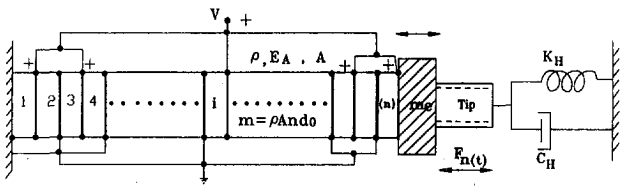

Fig. 5 Model of piezoelectric actuator for dynamic analysis with tip stiffness

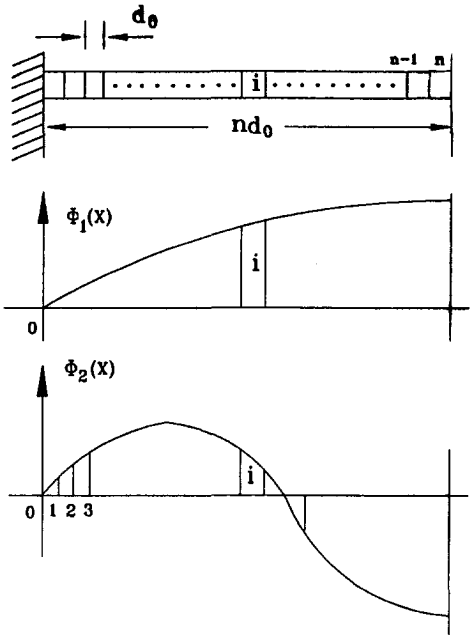

Fig. 6 The assumed mode shapes for axial deflection of the Piezo Stack

$$A_i = A, \quad d_{i0} = d_0, \quad E_{Ai} = E_A,$$

$$u_i(x, t) = u(x, t) = u, \quad d_{33_i} = d_{33}, \quad \rho_i = \rho \qquad (15)$$

According to Eq. (8), the elastic energy of the ith ceramic disk or plate is

$$V_{Ti} = \frac{1}{2} E_A A \int_{(i-1)d_0}^{id_0} (u_i'(x, t))^2 dx \qquad (16)$$

and the total elastic energy of the entire piezoelectric actuator is:

$$V_T = \sum_{i=1}^{n} V_{Ti} = \frac{1}{2} E_A A \sum_{i=1}^{n} \int_{(i-1)d_0}^{id_0} (u_i'(x, t))^2 dx$$

$$= \frac{1}{2} E_A A \int_0^{nd_0} (u'(x, t))^2 dx \qquad (17)$$

For each ceramic disk, the electrical energy is

$$W_{Ti} \doteq \frac{1}{2} \frac{q_i^2}{c_i(d_0)} \qquad (18)$$

and the total electric energy is then

$$W_T = \sum_{i=1}^{n} W_{Ti} = \frac{1}{2} \sum_{i=1}^{n} \frac{q_i^2}{c_i(d_0)} \qquad (19)$$

The coupling energy (electromechanical energy equation) Eq. (11) for each ceramic disk can be written as

$$Z_{Ti} = -d_{33_i} \frac{q_i}{c_i d_0} E_{A_i} A_i \int_{(i-1)d_0}^{id_0} u_i'(x, t) dx \qquad (20)$$

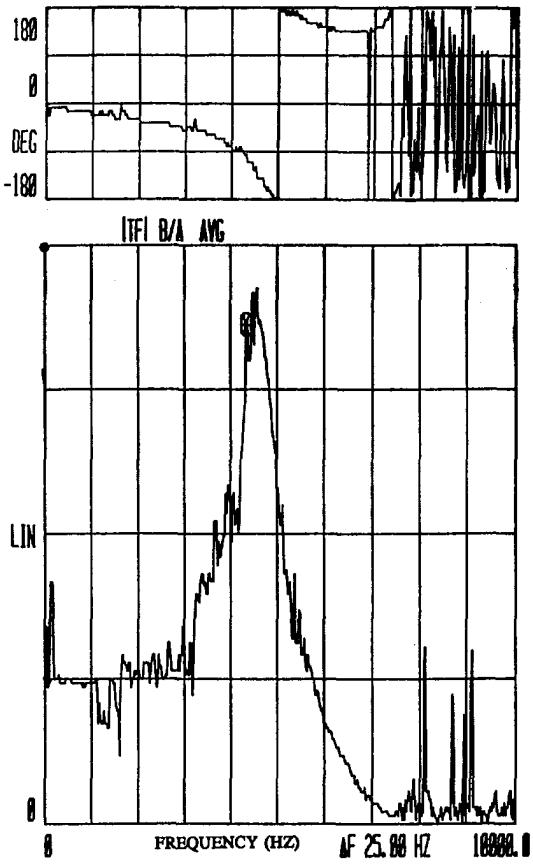

Fig. 7 The measured free tip transfer function of the piezoelectric actuator

By summing Eq. (20), the total coupling energy is

$$Z_T = -d_{33}E_A A \sum_{i=1}^{n} \frac{q_i}{c_i d_0} \int_{(i-1)d_0}^{id_0} u'(x, t)dx \qquad (21)$$

the kinetic energy of a ceramic disk or plate from Eq. (13) is

$$T_i = \tfrac{1}{2} \int_{(i-1)d_0}^{id_0} \rho_i A_i \dot{u}_i^2(x, t)dx \quad i = 0, \ldots, n-1 \qquad (22)$$

and the nth ceramic disk's kinetic energy is

$$T_n = \tfrac{1}{2} \int_{(n-1)d_0}^{nd_0} \rho_n A_n \dot{u}_n^2(x, t)dx + \tfrac{1}{2} m_e \dot{u}_n^2(x, t)|_{x=nd_0} \qquad (23)$$

Therefore, the total kinetic energy is

$$T_T = \sum_{i=1}^{n} T_i$$

$$= \tfrac{1}{2} \rho A \sum_{i=1}^{n} \int_{(i-1)d_0}^{id_0} \dot{u}_i^2(x, t)dx + \tfrac{1}{2} m_e \dot{u}_n^2(x, t)|_{x=nd_0} \qquad (24)$$

or

$$T_T = \tfrac{1}{2} \rho A \int_0^{nd_0} \dot{u}^2(x, t)dx + \tfrac{1}{2} m_e \dot{u}^2(nd_o, t) \qquad (25)$$

The Lagrange function of the electromechanical system is (Crandall, 1990)

$$\mathcal{L} = T_T - V_T - W_T - Z_T \qquad (26)$$

and the virtual work is

$$\delta W = -(F_n(t)\delta u_n(x, t) + C_H \dot{u}_n(x, t)\delta u_n)|_{x=nd_0} + \sum_{i=1}^{n} V_i \delta q_i$$

$$= (-K_H - C_H \dot{u}(x, t))\delta u(x, t)|_{x=nd_0} + \sum_{i=1}^{n} V_i \delta q_i \qquad (27)$$

where the electrical virtual work is defined by

$$\sum_{i=1}^{n} V_i \delta q_i \qquad (28)$$

Mode Approximation of the Piezoelectric Actuator

The longitudinal vibration of a piezoelectric actuator can be approximated by the finite mode superposition method. The response of vibration at location x can be expressed as

$$u(x, t) = \sum_{i=1}^{n} \Phi_i(x) w_i(t) \qquad (29)$$

For simplicity, two modes were assumed. The response of vibration at any location 'x' can then be represented

$$u(x, t) = \Phi_1(x) w_1(t) + \Phi_2(x) w_2(t) \qquad (30)$$

where two approximate modes are

$$\Phi_1(x) = \sin \frac{\pi x}{2nd_0}, \quad \Phi_2(x) = \sin \frac{3\pi x}{2nd_0} \qquad (31)$$

Figures 6(a, b, c) show the first two mode shapes. Differentiating Eq. (30) with respect to time t, gives

$$\dot{u}(x, t) = \Phi_1(x) \dot{w}_1(t) + \Phi_2(x) \dot{w}_2(t) \qquad (32)$$

and differentiating Eq. (30) with respect to x, gives

$$u'(x, t) = \Phi_1'(x) w_1(t) + \Phi_2'(x) w_2(t) \qquad (33)$$

By substituting Eqs. (32), and (33) into Eqs. (17), (21), (25), and (27), the energy equations for the stacked piezoelectric actuator model can be written as:

Potential energy

$$V_T = \frac{1}{2} \frac{\pi^2}{8} K_e(w_1^2(t) + 9w_2^2(t)) \qquad (34)$$

where

$$K_e = \frac{E_A A}{nd_0} \qquad (35)$$

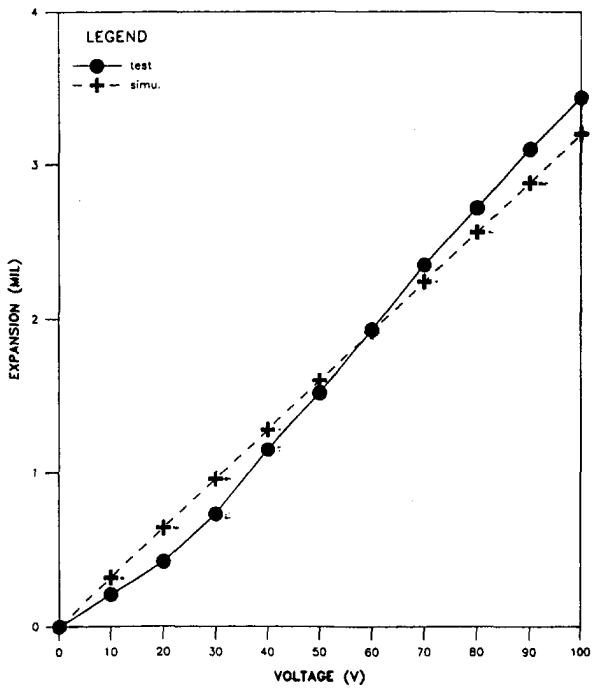

Fig. 8 Measured and simulated static expansion characteristics of subjected to a DC input voltage

Electromechanical coupling energy

$$Z_T = -\frac{d_{33}E_AA}{d_0}\sum_{1=1}^{n}\frac{q_i}{c_i}\int_{(i-1)d_0}^{id_0}(aw_1(t)\cos(ax) + 3w_2(t)a\cos(3ax))dx \quad (36)$$

Kinetic energy is

$$T_T = \tfrac{1}{2}(\tfrac{1}{2}m_e + m)(\dot{w}_1^2(t) + \dot{w}_2^2(t)) + \tfrac{1}{2}(-2m\dot{w}_1(t)\dot{w}_2(t)) \quad (37)$$

The virtual work can be written as

$$\delta W = -K_H(w_1(t) - w_2(t)) - C_H(\dot{w}_1(t) - \dot{w}_2(t))(\delta w_1 - \delta w_2) + \sum_{i=1}^{n} V_i\delta q_i \quad (38)$$

On substituting these Eqs. (34), (36), (38), and (19) in Eq. (26), the Lagrange function becomes;

$$\mathcal{L} = \frac{1}{2}\left(\frac{1}{2}m_e + m\right)(\dot{w}_1^2(t) + \dot{w}_2^2(t)) + \frac{1}{2}(-2m\dot{w}_1(t)\dot{w}_2(t)) - \frac{1}{2}\frac{\pi^2}{8}k_e(w_1^2(t) + 9w(t) - 2^2) - \frac{1}{2}\sum_{i=1}^{n}\frac{q_i^2}{c_i} + \frac{d_{33}E_AA}{d_0}\sum_{i=1}^{n}\frac{q_i}{c_i}\int_{(i-1)d_0}^{id_0}(aw_1(t)\cos(ax) + 3aw_2(t)\cos(3ax))dx \quad (39)$$

The Lagrange's equation is given by

$$\frac{d}{dt}\left(\frac{\partial\mathcal{L}}{\partial\dot{w}_i}\right) - \frac{\partial\mathcal{L}}{\partial w_i} = -K_Hw_i - C_H\dot{w}_i \quad (i = 1, 2) \quad (40)$$

and

$$\frac{d}{dt}\left(\frac{\partial\mathcal{L}}{\partial\dot{q}_i}\right) - \frac{\partial\mathcal{L}}{\partial q_i} = V_i \quad (i = 1, 2, \ldots, n) \quad (41)$$

Assume that the voltage and charge on each disc are the same

$$V_i = V, \quad q_i = q \quad (42)$$

and that each disk has the same capacitance as evaluated with zero force and voltage applied, $c_i = c_0$. The responses of the system will have the same form as the external voltage source, i.e.,

$$q(t) = \bar{Q}e^{j\omega t}, \quad V(t) = \bar{V}(j\omega)e^{j\omega t}, \quad w_1(t) = \bar{W}_1(j\omega)e^{j\omega t}, \quad w_2(t) = \bar{W}_2(j\omega)e^{j\omega t} \quad (43)$$

Equation (40) can now be written as

$$\left(\frac{1}{2}m_e + m\right)\ddot{w}_1 + C_H\dot{w}_1 + \left(\frac{\pi^2}{8}K_e + K_H\right)w_1 - (m\ddot{w}_2 + C_H\dot{w}_2 + K_Hw_2) - \frac{d_{33}E_AA}{d_0C_0}q = 0$$

$$\left(\frac{1}{2}m_e + m\right)\ddot{w}_2 + C_H\dot{w}_2 + \left(\frac{9\pi^2}{8}K_e + K_H\right)w_2 - (m\ddot{w}_{1_1} + C_H\dot{w}_1 + K_Hw_1) + \frac{d_{33}E_AA}{d_0C_0}q = 0 \quad (44)$$

and Eq. (41) becomes

$$n\frac{q}{c_0} = nV + \frac{d_{33}E_AA}{d_0c_0}(w_1 - w_2) \quad (45)$$

Applying Eq. (43) to the above three equations, yields

$$\begin{pmatrix} \left(\frac{\pi^2}{8}K_e + K_H\right) & -(K_H - m\omega^2 + jC_H\omega) & -\frac{d_{33}E_AA}{d_0c_0} \\ -(\tfrac{1}{2}m_e + m)\omega^2 & & \\ -(K_H - m\omega^2 + jC_H\omega) & \left(\frac{9\pi^2}{8}K_e + K_H\right) & \frac{d_{33}E_AA}{d_0c_0} \\ & -(\tfrac{1}{2}m_e + m)\omega^2 + jC_H\omega & \\ -\frac{d_{33}E_AA}{nd_0c_0} & \frac{d_{33}E_AA}{nd_0c_0} & \frac{1}{c_0} \end{pmatrix}\begin{pmatrix} \bar{W}_1(j\omega) \\ \bar{W}_2(j\omega) \\ \bar{Q}(j\omega) \end{pmatrix} = \begin{pmatrix} 0 \\ 0 \\ \bar{V}(j\omega) \end{pmatrix} \quad (46)$$

The transfer function between the tip displacement and applied (input) voltage is obtained by combining Eqs. (30) and (45) to obtain

$$G_{\text{piezo}}(j\omega) = \frac{\bar{U}(j\omega)}{\bar{V}(j\omega)} = \frac{(1.25\pi^2K_e - m_e\omega^2)d_{33}K_en}{\Delta(j\omega)} \quad (47)$$

The transfer function is defined as the ratio of the actuator tip displacement to the input control voltage. The actuator tip displacement is

$$U(nd_0, t) = w_1(t) - w_2(t) \quad (48)$$

Using Eqs. (44), Eq. (47) can be written as

$$U(nd_0, t) = \bar{U}(j\omega)e^{j\omega t} \quad (49)$$

and

$$\Delta(j\omega) = \left(\frac{\pi^2}{8}K_e + K_H - \left(\frac{1}{2}m_e + m\right)\omega^2 + jC_H\omega\right) \times \left(\frac{9}{8}\pi^2 K_e + K_H - \left(\frac{1}{2}m_e + m\right)\omega^2 + jC_H\omega\right) - (K_H - m\omega^2 + jC_H\omega)^2 \quad (50)$$

and the piezoelectric charge constant is related to the expansion, external DC voltage, and number of piezoelectric plates as

$$d_{33} = \frac{\delta}{Vn} \quad (51)$$

Correlation of Analytical and Test Results for the Piezoelectric Actuator

Figure 7 shows the measured transfer function (ratio of tip displacement to the input voltage) for the piezoelectric actuator. Figure 8 shows the measured and simulated static expansion characteristics of the actuator subjected to an external DC voltage. The product of the piezoelectric charge constant and number of the piezoelectric plates ($d_{33}n$) can be identified by Eq. (51) and the test results in Fig. 8. The expansion under the 100 V DC voltage is 3.5 mil. Hence $d_{33}n$ can be obtained as

$$d_{33}n = \frac{\delta}{V} = \frac{3.5 \times 0.0254 \times 10^{-3}}{100} = 9.0E - 7\ m/v \quad (52)$$

The actuator's other physical parameters are obtained from the manual and measurement. These parameters are specified below:

$$K_e = 33E + 6\ \text{N/m}$$
$$K_H = 15E + 6\ \text{N/m}$$
$$m = 0.09\ \text{kg}$$
$$m_e = 0.023\ \text{kg}$$
$$C_H = 500N\ \text{s/m}$$

On substituting the above parameters into Eq. (46), the transfer function becomes

$$G_{\text{piezo}}(j\omega) = \frac{5.2E - 7 + 2.8E - 17(j\omega)^2}{1 + 8.843E - 6j\omega + 1.784E - 9(j\omega)^2 + 4.35E - 16(j\omega)^3 + 8.26E - 20(j\omega)^4} \quad (53)$$

Figure 9 shows the transfer function comparison between simulation and measured data. Good agreement was achieved in amplitude at resonance when a reasonable amount of external damping (C_H = 500 N-s/m) was used in (53).

Hydraulic Actuator Dynamic Model

An accurate dynamic model of a hydraulic actuator is difficult to obtain, due to the effects of the pipe or tube material, geometry, fluid properties, assembling and mounting conditions, etc. The transfer function matrix measurement method can be used for identifying this model. Figure 10 represents the relation between input force, input displacement and output force. Output displacement and force are obtained from

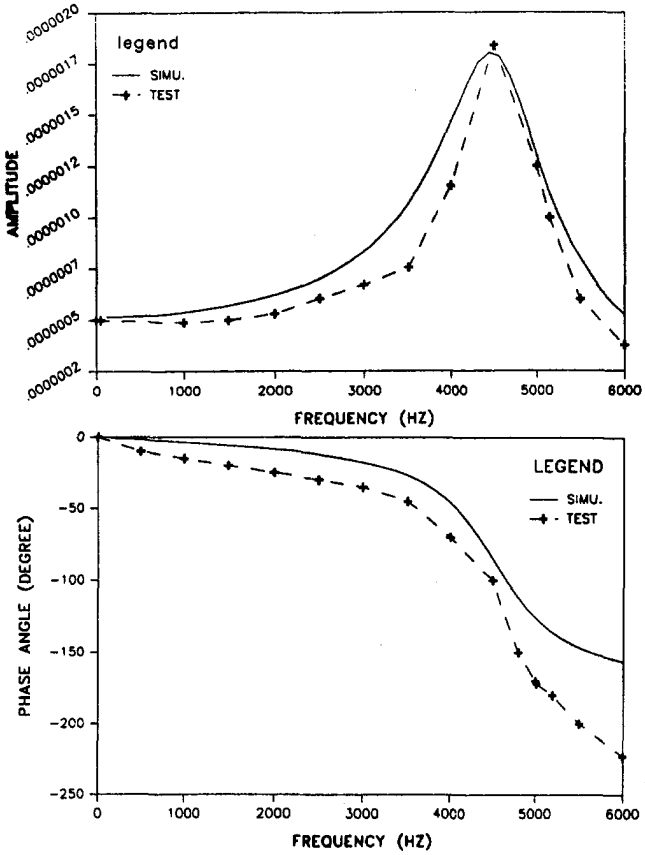

Fig. 9 The transfer function comparison of simulation with test for piezoelectric actuator

$$\begin{pmatrix} F_{\text{out}}(s) \\ X_{\text{out}}(s) \end{pmatrix} = \begin{pmatrix} H_{11}(s) & H_{12}(s) \\ H_{21}(s) & H_{22}(s) \end{pmatrix} \begin{pmatrix} F_{\text{in}}(s) \\ X_{\text{in}}(s) \end{pmatrix} \quad (54)$$

or

$$\begin{pmatrix} F_{\text{out}}(s) \\ X_{\text{out}}(s) \end{pmatrix} = H \begin{pmatrix} F_{\text{in}}(s) \\ X_{\text{in}}(s) \end{pmatrix} \quad (55)$$

By inverting matrix H, Eq. (54) can be written as

$$\begin{pmatrix} F_{\text{in}}(s) \\ X_{\text{in}}(s) \end{pmatrix} = \begin{pmatrix} G_{11}(s) & G_{12}(s) \\ G_{21}(s) & G_{22}(s) \end{pmatrix} \begin{pmatrix} F_{\text{out}}(s) \\ X_{\text{out}}(s) \end{pmatrix} \quad (56)$$

or

$$\begin{pmatrix} F_{\text{in}}(s) \\ X_{\text{in}}(s) \end{pmatrix} = G \begin{pmatrix} F_{\text{out}}(s) \\ X_{\text{out}}(s) \end{pmatrix} \quad (57)$$

where

$$\begin{pmatrix} G_{11}(s) & G_{12}(s) \\ G_{21}(s) & G_{22}(s) \end{pmatrix} = \begin{pmatrix} H_{11}(s) & H_{12}(s) \\ H_{21}(s) & H_{22}(s) \end{pmatrix}^{-1} \quad (58)$$

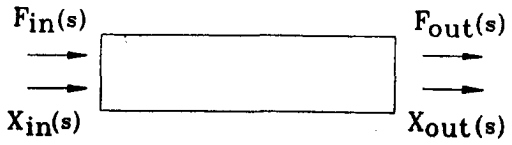

Fig. 10 Hydraulic actuator transfer variables

from Eq. (56)

$$X_{in}(s) = G_{21}F_{out}(s) + G_{22}(s)X_{out}(s) \tag{59}$$

The $G_{21}(s)$, and $G_{22}(s)$ are obtained by employing the following boundary conditions

$$G_{21} = \left.\frac{X_{in}(s)}{F_{out}(s)}\right|_{X_{out}(s)=0} \tag{60}$$

and

$$G_{22}(s) = \left.\frac{X_{in}(s)}{X_{out}(s)}\right|_{F_{out}(s)=0} \tag{61}$$

then the output force $F_{out}(s)$ is obtained from equation (59) and is given as

$$F_{out}(s) = G_{21}^{-1}(s)(X_{in}(s) + G_{22}(s)X_{out}(s)) \tag{62}$$

Equation (62) is represented as a flow diagram in Fig. 11, where $x^*(s)$ is rotor motion, and $x_{in}(s)$ is the input piston displacement or piezoelectric actuator tip displacement. It is obvious that the output force to rotor is coupled by the input and output displacements. In other words, the output force is determined by the hydraulic actuator, piezoelectric actuator, and rotor motions. Equation (62) also provides a convenient approach in assembling the closed loop model. $G_{21}^{-1}(s)$ can be identified by the following enforced boundary equation

$$G_{21}^{-1}(s) = \left.\frac{F_{out}(s)}{X_{in}(s)}\right|_{X_{out}(s)=0} \tag{63}$$

Equations (60) and (61) can be rewritten as follows

$$G_{21}^{-1}(s) = \left(\frac{X_{in}(s)}{F_{out}(s)}\right)^{-1}_{X_{out}(s)=0} = \left.\frac{\beta_{in}V_{out}(s)}{\alpha_{force}V_{in}(s)}\right|_{X_{out}(s)=0} \tag{64}$$

and

$$G_{22}(s) = \left.\frac{X_{in}(s)}{X_{out}(s)}\right|_{F_{out}(s)=0} = \left.\frac{\beta_{out}V_{in}(s)}{\beta_{in}V_{out}(s)}\right|_{F_{out}(s)=0} \tag{65}$$

where:

β_{out}	sensitivity of output displacement probe (9960 V/m)
β_{in}	sensitivity of input displacement probe (7559 V/m)
α_{force}	sensitivity of output force gauge (7.225*E*-3 *V/N*)
$V_{Fout}(s)$	analog signal of output force gauge (*V*)
$V_{out}(s)$	analog signal of output displacement probe (*V*)
$V_{in}(s)$	analog signal of input displacement probe (*V*)

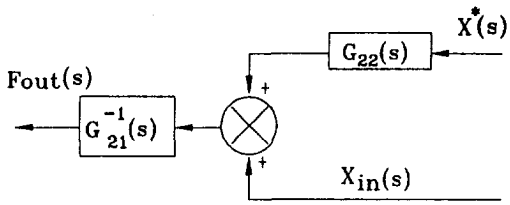

Fig. 11 Flow diagram of the transfer Eq. (62)

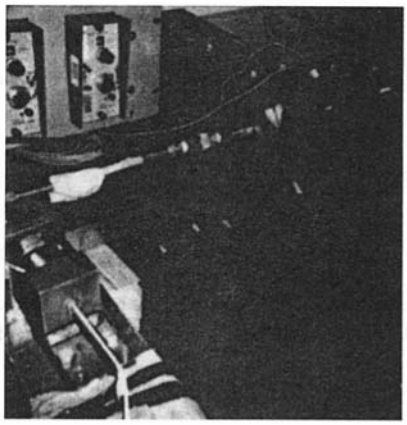

Fig. 12 Hydraulic actuator transfer function matrix measurement setup (input probe and piezoelectric actuator)

Therefore, Eqs. (64) and (65) can be written as

$$G_{21}^{-1}(s) = \left(\frac{X_{in}(s)}{F_{out}(s)}\right)^{-1}_{X_{out}(s)=0} = 1.046\ 10^{6}\left(\frac{V_{F_{out}}(s)}{V_{in}(s)}\right)_{X_{out}(s)=0}$$

$$= \frac{1.36\ 10^{6} + 8.726s}{1 + 1.285\ 10^{-4}s - 1.2638\ 10^{-8}s^{2}} \tag{66}$$

and

$$G_{22}(s) = \left(\frac{\beta_{out}V_{in}(s)}{\beta_{in}V_{out}(s)}\right)_{F_{out}(s)=0} = 1.32\left(\frac{V_{in}(s)}{V_{out}(s)}\right)_{F_{out}(s)=0}$$

$$= -\frac{0.42 + 1.18910^{-3}s}{1 + 1.04110^{-3}s - 4.8610^{-7}s^{2}} \tag{67}$$

Figures 12 and 13 show the photos of the setup for measurement of transfer functions which are represented in Eqs. (66) and (67). There are two Bently probes (input piston probe and output piston probe) and one force gauge in the measurement setup. The input probe was used in sensing the input piston displacement through a extension bar which was set between the input piston and piezoelectric actuator tip. The output piston probe which was mounted in a fixed block was used directly in measuring the output piston displacement. A force gauge was employed in obtaining the output force. The measurement setup to satisfy the boundary condition in Eq. (66) is to fix the output piston against the force gauge face which was mounted on the wall of the fixed block. The transfer function in Eq. (66) can

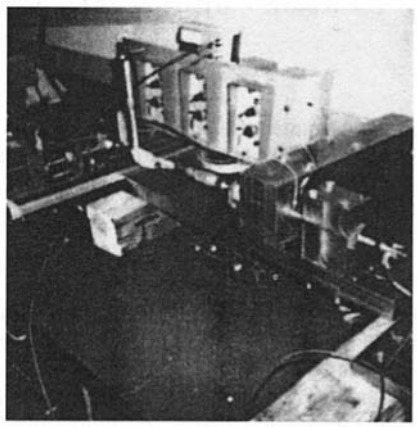

Fig. 13 Hydraulic actuator transfer function matrix measurement setup (output probe and force gauge)

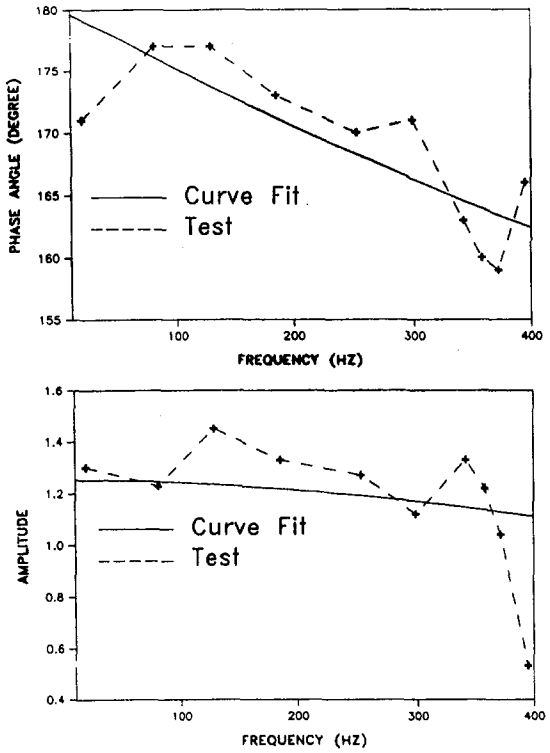

Fig. 14 Curve fit-measurement comparison for $G_{21}^{-1}(s)$

be obtained by the analysis of force signal and input piston signal. In similar way, the setup to satisfy the boundary condition in Eq. (67) is to set the output piston against a very small spring stiffness. The transfer function in Eq. (67) can be obtained from the input piston displacement and output piston displacement signals.

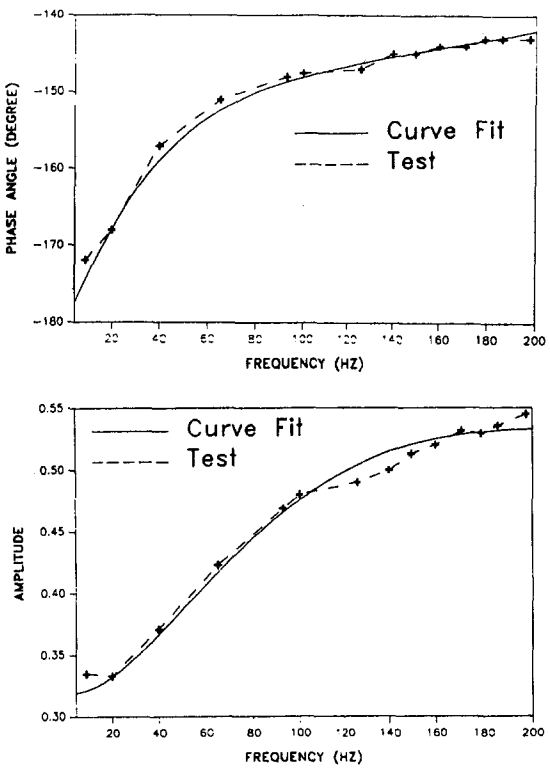

Fig. 15 Curve fit-measurement comparison for $G_{22}(s)$

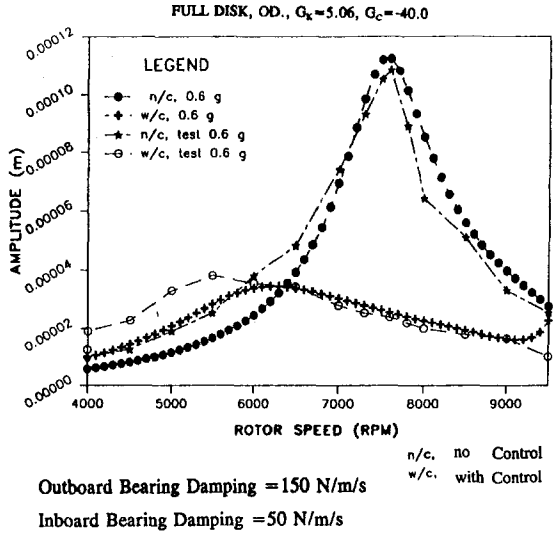

Fig. 16 Application of active vibration control simulation with electromechanical modeling of the piezohydraulic actuator

Figures 14 and 15 are the curve fits for $V_{Fout}(s)/V_{in}(s)$ and $V_{in}(s)/V_{out}(s)$, respectively. The test result in Fig. 14 could be curve fitted by a higher order model. However, a second-order transfer function model (see Eq. (66)) was employed for sake of illustration. The piezoelectric actuator was used for the active vibration control of an air turbine driven test rotor at NASA Lewis. This application is described in Lin (1991) and Palazzolo (1991a, 1991b). An electromechanical model was constructed for the flexible rotor/shaft, PD controller and piezohydraulic actuators (4). The theoretical and measured vibration amplitude vs. rotor speed curve are shown in Fig. 16, for the case of traversing a critical speed.

Summary

The electromechanical dynamic model of the piezohydraulic actuator system was developed. An electromechanical energy based method was employed in the piezoelectric ceramic disk or plate to get the total energy of a stacked piezoelectric actuator. A fourth-order model was used in obtaining the transfer function of the piezoelectric actuator between its input voltage and output displacement. This model may be assembled into the closed loop dynamic simulation. Good agreement was achieved between simulation and test results. Transfer matrix components for the hydraulic actuator were identified by shaking the actuator with special boundary conditions. The output force of the hydraulic actuator was represented by a linear combination of the input and output displacement transfer function components. Good correlation of test and simulation for a rotor test rig with piezo-hydraulic actuator based AVC was included.

Acknowledgments

The authors thank NASA Lewis and the U.S. Army at NASA Lewis for funding this research, and Dr. Wenduan Li for preparing the liquid plastic employed in the hydraulic actuator.

References

Cade, Waller Cuyton, 1946, *Piezoelectricity: An Introduction to the Theory and Applications of Electromechanical Phenomena in Crystals,* McCraw-Hill, New York, NY.

Crandall, S. H., et al., 1990, *Dynamics of Mechanical and Electromechanical Systems,* McGraw-Hill, New York, NY, pp. 371–389.

Holland, R., et al., 1968, "Resonant Properties of Piezoelectric Ceramic Rectangular Parallelepipeds," *J. Acoust. Soc. Am.,* Vol. 43, pp. 988–997.

Kossoff, G., 1966, "The Effects of Backing and Matching on the Performance of Piezoelectric Ceramic Transducer," *IEEE Trans. Son. Ultrason.,* Vol. SU-13, pp. 259–263.

Lin, R. R., Palazzolo, A. B., Kascak, A. F., and Montague, G. T., 1991, "Electromechanical Simulation and Testing of Actively Controlled Rotordynamic Systems with Piezoelectric Actuators," *Proceedings of International Gas Turbine Conference,* Orlando, FL, June 3–6, accepted for publication in the *Trans.* ASME.

Lin, R. R., 1990, "Active Vibration Control of Rotorbearing Systems Utilizing Piezoelectric Pushers," Ph.D. dissertation, Texas A&M University, Texas, pp. 49–50.

Palazzolo, A. B., Lin, R. R., Alexander, R. M., Kascak, A. F., and Montague, G., 1991a, "Test and Theory for Piezoelectric Actuator-Active Vibration Control of Rotating Machinery," ASME *Journal of Vibration and Acoustics,* Apr. Vol. 113, pp. 167–175.

Palazzolo, A. B., Jagannathan, S., Kascak, A. F., Montague, G., and Kiraly, L. J., 1991b, "Hybrid Active Vibration Control of Rotorbearing Systems Using Piezoelectric Actuators," *Proceedings of ASME 13th Biennial Conference on Mechanical Vibration,* Miami, FL, Sept. 22–25.

Tang, P., Palazzolo, A. B., Kascak, S., and Montague, A. F., 1993a, "A Combined Piezoelectric-Hydraulic Actuator Based on Active Vibration," presented to the 14th Biennial Conference on Mechanical Vibration and Noise, Albuquerque, Sept. 19–22, and to ASME Journal of Acoustics and Vibration.

Tang, P., and Palazzolo, A. B., et al., 1993b, "Electro-Mechanical Simulation for a Rotor Test Rig with a Cryogenic Magnetic Bearing," presented to 1993 ASME TURBO EXPO May 24–27, 1993, and submitted to ASME JOURNAL OF DYNAMIC SYSTEMS, MEASUREMENT, AND CONTROL.

Tomikawa, Y., and Miura, M., 1978, "Analysis of Electrical Equivalent Circuit Elements of Piezo-tuning Forks by the Finite Element Method," *IEEE Trans. Son. Ultrason.,* Vol. SU-25, pp. 206–212.